POLITECNICO DI TORINO
Repository ISTITUZIONALE

C0 beam elements based on the Refined Zigzag Theory for multilayered composite and sandwich laminates

Availability:
This version is available at: 11583/2424723 since:

(Article begins on next page)

14 January 2025

C0 beam elements based on the Refined Zigzag Theory for multilayered composite and sandwich laminates

Marco Gherlone [a,*], Alexander Tessler [b], Marco Di Sciuva [a]

a Department of Aeronautics and Space Engineering, Politecnico di Torino, Corso Duca degli Abruzzi 24, 10129 Torino, Italy

b Structural Mechanics and Concepts Branch, NASA Langley Research Center, Mail Stop 190, Hampton, VA 23681-2199, USA

1. Introduction

Laminated composite structures have been used increasingly over the past forty years in military and civilian aircraft, aerospace vehicles, naval and civil structures. Offering extensive tailoring capabilities to suit specific load paths, high stiffness-to-weight and strength-to-weight ratios, these man-made materials have also proven to provide major economic and environmental advantages over the traditional metallic structures. When applied to primary load-bearing structures, the multilayered, sandwich, and relatively thick-section composites are required. Such structures are known to exhibit higher-order deformation effects due to transverse shear and normal stresses and strains, thus requiring advanced design and analysis methods that adequately take into account these higher-order effects.

It is well established that Bernoulli–Euler (classical) and Timoshenko [1] beam theories are not well-suited for the analysis of laminated composite and sandwich beams. This is because neither theory has the sufficient kinematic freedom to accommodate the complex cross-sectional distortions associated with the bending and axial-to-bending coupling deformations. By including an additional kinematic variable – the average bending rotation – Timoshenko theory accommodates transverse shearing of the cross-section; however, an average corrective strategy that calls for a *shear-correction factor* is used to correct the erroneous assumption of constant transverse shear strain through the depth of the beam [2]. The adoption of a suitable shear-correction factor often yields relatively accurate predictions of deflection and lowest natural frequencies; however, especially for laminated composite and sandwich cross-sections, Timoshenko theory fails to obtain adequate solutions for the important design quantities such as the peak values of axial stresses and strains.

Improvements to the classical theories have been obtained by: (1) Equivalent Single Layer (ESL) theories that assume a priori

the behavior of the unknowns (displacements and/or stresses) through the laminate thickness, and (2) Layer-Wise (LW) theories, in which the distribution of the unknowns is assumed layer by layer. ESL theories are generally computationally efficient; however, they often produce inaccurate through-the-depth distributions of strains and stresses, particularly the transverse-shear stresses and strains. The LW theories are usually sufficiently accurate; however, the number of unknowns is proportional to the number of material layers, and for multilayered composite laminates the computational effort is generally prohibitively expensive, especially for large-scale models.

An attractive compromise between the accuracy of LW theo-ries and the computational efficiency of ESL theories is repre-sented by the so-called zigzag theories. In this class of theories, the axial displacement field is a superposition of a zigzag-like dis-tribution through-the-depth and linear or cubic ESL-like "smeared" distributions. The resulting theories are respectively referred to as the linear and cubic zigzag theories. These theories ensure a fixed number of kinematic variables regardless of the number of material layers. The zigzag kinematic distributions are constructed in such a way as to ensure through-the-depth continuous transverse-shear stresses, that are constant for linear theories and piecewise parabolic for cubic theories. Zigzag theo-ries thus provide accurate response predictions for relatively thick laminated-composite and sandwich structures and yield response predictions comparable to those of computationally intensive LW theories (e.g., refer to Reddy [3]).

Averill developed the linear [4] and cubic [5] zigzag beam the-ories by using Timoshenko theory as a baseline and by introducing an independent kinematic variable associated with the zigzag kinematics. This strategy allows the use of C^0-continuous deflec-tion interpolations instead of the C^1-continuous deflection required in Di Sciuva and related theories [6–12]. Averill also enforces a con-tinuous transverse-shear stress through the laminate thickness using an exterior penalty formulation. The realization of the erro-neously vanishing transverse-shear stress at a clamped boundary prompted Averill to abandon the use of the variationally required kinematic boundary conditions.

Tessler et al. [13–20] recently developed the Refined Zigzag Theories (RZT) for beams and plates that, in a manner similar to Averill, adopt Timoshenko (for beams) and FSDT (for plates) kinematic assumptions as their baseline; the components of the inplane displacements are enhanced by the addition of piece-wise-linear (i.e., zigzag) functions that have a novel mathematical description. In contrast to the previous zigzag-theory attempts including those by Averill [4,5] – in which zigzag functions are designed to vanish in an arbitrarily specified layer – these new zigzag functions have the property of vanishing on the top and bottom surfaces of a laminate. As a further departure from the previous efforts, the transverse-shear stresses are not required to be continuous across the layer interfaces, resulting in the piecewise-constant functions that provide sufficiently accurate estimates of the true shear-stress distributions. The equilibrium equations, constitutive equations, boundary conditions, and strain–displacement relations are consistently derived from the virtual work principle without engendering any transverse-shear stress (force) anomalies. The resulting transverse-shear stresses and forces are fully consistent with respect to the physical and variational requirements and they do not vanish erroneously along clamped boundaries. Moreover, the RZT theories yield con-sistently superior results over a wide range of aspect ratios and material systems, including thick laminates with a high degree of transverse shear flexibility, anisotropy, and heterogeneity. A particularly appealing aspect of RZT for application to the finite element method is that its kinematic variables need not exceed

C^0 continuity, thus the possibility for developing simple and effi-cient finite element.

Although computational desirable and most-widely used in commercial finite-element software, C^0-continuous bending ele-ments can exhibit excessively stiff behavior when applied to rela-tively thin structural members – the phenomenon commonly referred to as *shear locking*. When the full quadrature (exact inte-gration) is used to compute the strain energy, Timoshenko ele-ments based on the linear isoparametric shape functions (as well as similar FSDT plate elements) exhibit severe shear locking in the thin bending regime. The *reduced* integration of the transverse shear energy has been shown to be effective to alleviate shear lock-ing; however, when applied to plate elements [21], the reduced integration elements engender the non-physical zero-energy modes which require special suppression techniques to be useful for practical applications. The use of higher-order polynomials gen-erally improves thin-regime predictions; however, the rate of con-vergence is commonly diminished. Several other successful approaches dealing with the shear-locking issues have been ad-vanced which include the discrete penalty constraints, penalty-relaxation parameters, rotational bubble modes, and *anisoparamet-ric* interpolations (the terms *interdependent* and *linked* interpola-tions have also been used); refer to [22,23] for the technical details on these techniques and related literature. The *anisopara-metric* interpolation strategy, advanced by Tessler and co-workers, for beam, plate, and shell elements (e.g., refer to [24–38]), requires the deflection variable to be interpolated with a complete polyno-mial one degree higher than the bending rotation variables (*aniso-parametric* element). To achieve simple, isoparametric-like nodal patterns, the higher-order shear strain terms are set to zero by way of *continuous* shear constraints, thus eliminating the extra deflection degrees-of-freedom (*constrained anisoparametric* ele-ment). The resulting elements are simple, computationally effi-cient, and variationally consistent. In the case of the *constrained anisoparametric* two-node beam element [24], it was shown that its stiffness matrix is identical to that of the linear isoparametric element whose transverse-shear strain energy is obtained by *re-duced* integration [21]. The major advantage of the *anisoparametric* elements is that all energy integrations are performed with the full Gaussian quadrature to maintain the required variational consis-tency; furthermore, the resulting consistent load and mass matri-ces give rise to superior predictions over the comparable reduced integration elements, producing elements of improved accuracy [21,23].

In this paper, the Refined Zigzag Theory for multilayered com-posite and sandwich beams is used to derive a set of simple and efficient three- and two-node C^0-continuous *anisoparametric* beam elements (several formulations for the RZT-based beam and plate elements were initially explored in [39,40]). The analytic theory is first reviewed to establish the framework for the finite element development, and to ascertain the predictive capability of the the-ory for composite and sandwich laminates in cylindrical bending. The choice of suitable shape functions is then addressed with a specific focus on the shear-locking issues and their consistent res-olution within the variational requirements. Three different con-straint strategies are examined to derive three types of two-node *constrained anisoparametric* elements that do not exhibit any path-ological stiffening when modeling slender beams (i.e., no shear locking). Computational studies with simply supported and canti-levered beams are performed to establish the elements' conver-gence characteristics and predictive capabilities for relatively deep (thick) and very slender (thin) composite and sandwich beams. The numerical results confirm that the two-node element derived on the basis of a constant shear-force constraint is the best performing *constrained anisoparametric* element.

2. A brief review of Refined Zigzag Theory for beams

In this section, the basic assumptions of the new Refined Zigzag Theory for composite and sandwich beams are reviewed and the equations necessary for the subsequent finite element development are derived. For the additional technical details on the theory, refer to [14,15].

2.1. Displacements, zigzag kinematics, strains, and stresses

Consider a beam of length L, and cross-sectional area $A = 2h \times b$ made of N orthotropic material layers that are perfectly bonded to each other (Fig. 1); each layer is denoted by the superscript (k). The beam is referred to the Cartesian coordinate system (x, y, z), where $x \in [x_a, x_b]$ denotes the beam longitudinal axis, and $z \in [-h, h]$ the thickness coordinate. The thickness of the kth layer is $2h^{(k)}$(Fig. 2a). Only planar deformations in the (x, z) plane are consid-ered under the static loading which includes the distributed axial,
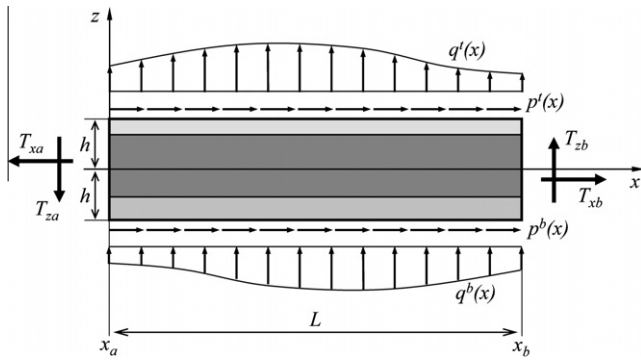

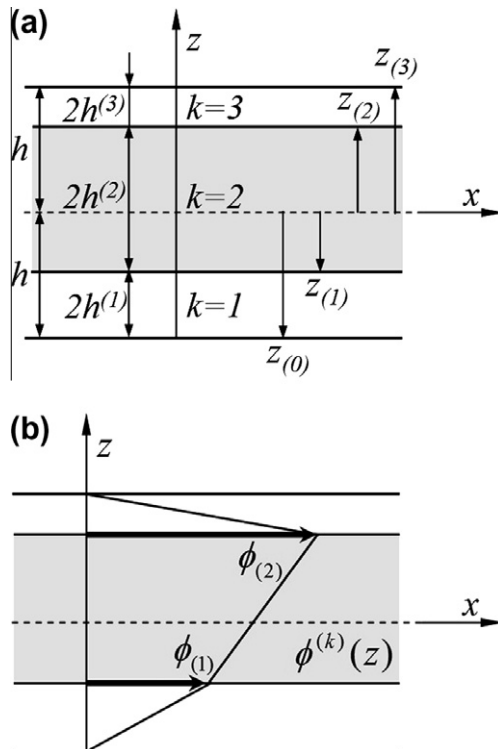**Fig. 1.** Notation for beam geometry and applied loading.

Fig. 2. Through-thickness layer notation and zigzag function of the Refined Zigzag Theory for a three-layered laminate: (a) layer notation and (b) zigzag function.

$p^b(x)$ and $p^t(x)$, and transverse, $q^b(x)$ and $q^t(x)$, loads (units of force/length) applied at the bottom ($z = -h$) and top ($z = +h$) beam surfaces. In addition, the end cross-sections are subject to the prescribed axial (T_{xa}, T_{xb}) and transverse shear (T_{za}, T_{zb}) tractions.

The orthogonal components of the displacement vector are defined as

$$\begin{Bmatrix} u_x^{(k)}(x,z) \\ u_z(x,z) \end{Bmatrix} = \begin{bmatrix} 1 & 0 & z & \phi^{(k)} \\ 0 & 1 & 0 & 0 \end{bmatrix} \begin{Bmatrix} u(x) \\ w(x) \\ \theta(x) \\ \psi(x) \end{Bmatrix} \equiv \mathbf{N_z u} \tag{1}$$

where $u_x^{(k)}$ and u_z are the displacements in the directions of the x- and z-axis, respectively, and $\mathbf{u}$ is a vector containing the four kinematic variables of the theory. Note that $u_z = w(x)$ is uniform across the depth of the beam, hence the superscript (k) does not appear in the notation for this quantity. The kinematic variables are the uniform axial displacement, $u(x)$, the deflection, $w(x)$, the average cross-sectional (bending) rotation, $\theta(x)$, and the zigzag rotation, $\psi(x)$. This additional variable, which does not appear in Timoshenko theory, serves the role of adjusting the magnitude of the total zigzag displacement, $\phi^{(k)}\psi(x)$, which is responsible for the modeling of cross-sectional distortion.

The zigzag function, $\phi^{(k)} \equiv \phi^{(k)}(\zeta^{(k)}, h^{(k)}, G_{xz}^{(k)}, G)$, has units of length, is a piecewise linear, C^0-continuous function of the thickness coordinate; $\phi^{(k)}$ is also lamination and material dependent, where the $\zeta^{(k)}$, $h^{(k)}$, $G_{xz}^{(k)}$ and G quantities will be defined subsequently. The $\phi^{(k)}$ function is defined in terms of its layer-interface values $\phi_{(i)}(i = 0, 1, \ldots, N)$ such that the homogeneous conditions on the top and bottom beam surfaces are identically satisfied (see Fig. 2b depicting the notation for a three-layered laminate), i.e.,

$$\phi^{(1)}(-h) = \phi_{(0)} = 0, \quad \phi^{(N)}(+h) = \phi_{(N)} = 0 \tag{2}$$

Thus, for the kth material layer located in the range $[z_{(k-1)}, z_{(k)}]$, the zigzag function is given by the linear polynomial

$$\phi^{(k)} \equiv \frac{1}{2}(1 - \zeta^{(k)})\phi_{(k-1)} + \frac{1}{2}(1 + \zeta^{(k)})\phi_{(k)}, \tag{3}$$

where $\zeta^{(k)} \in [-1, 1]$ is the local, kth layer thickness coordinate defined as

$$\zeta^{(k)} = [(z - z_{(k-1)})/h^{(k)} - 1] \quad (k = 1, \ldots, N) \tag{4}$$

The first layer begins at $z_{(0)} = -h$, the last N th layer ends at $z_{(N)} = h$, and the k th layer ends at $z_{(k)} = z_{(k-1)} + 2h^{(k)}$, where $2h^{(k)}$ denotes the kth layer thickness (Fig. 2a).

$$\phi_{(k)} = \phi_{(k-1)} + 2h^{(k)}\phi_{,z}^{(k)}, \quad \phi_{,z}^{(k)} = G/G_{xz}^{(k)} - 1 \quad (k = 1, \ldots, N) \tag{5}$$

In Eq. (5) G denotes a weighted-average transverse shear modulus of the total laminate given by

$$G = \left(\frac{1}{2h}\int_{-h}^{h}\frac{dz}{G_{xz}^{(k)}}\right)^{-1} = \left(\frac{1}{h}\sum_{k=1}^{N}\frac{h^{(k)}}{G_{xz}^{(k)}}\right)^{-1} \tag{6}$$

where $G_{xz}^{(k)}$ is the k th layer transverse shear modulus. The complete derivation of Eqs. (2)–(6) can be found in [15], and the approach is also applicable for plates [17–20].

An examination of Eqs. (5) and (6) reveals that for the case of homogeneous, single-layer beams, the zigzag function $\phi^{(k)}$ vanishes identically and the displacement field, Eq. (1), degenerates to that of Timoshenko theory. Tessler et al. [19,20] recently showed that, by adopting a novel strategy called the Homogeneous-Limit Modelling (HLM), the full power of zigzag kinematics in Eq. (1) can be exploited even for homogeneous cross-sections, resulting in the RZT capable of predicting highly accurate response quanti-ties including the strains and stresses. The approach constructs a multilayered cross-section whose material layers differ in their

transverse shear properties only infinitesimally. This strategy, in effect, achieves a homogeneous cross-section by forcing the kinematics into an infinitesimally small heterogeneous behaviour.

Adopting the linear strain–displacement relations of elasticity theory, the RZT strains become

$$
\begin{Bmatrix} \varepsilon_x^{(k)} \\ \gamma_{xz}^{(k)} \end{Bmatrix} = \begin{bmatrix} 1 & 0 & 0 & 0 & z & \phi^{(k)} \\ 0 & 1 & 1 & \beta^{(k)} & 0 & 0 \end{bmatrix} \begin{Bmatrix} u_{,x} \\ w_{,x} \\ \theta \\ \psi \\ \theta_{,x} \\ \psi_{,x} \end{Bmatrix}
\tag{7}
$$

where $\beta^{(k)} \equiv \phi_{,z}^{(k)}$ is a piecewise-constant function already defined in Eq. (5).

Within the assumptions that (i) each material layer is linearly elastic and orthotropic with the orthotropy axes corresponding to the Cartesian coordinates, (ii) the beam exhibits the plane-stress behavior in the (x, z) plane, and (iii) the transverse normal stress $\sigma_z^{(k)}$ is negligibly small compared to the axial and transverse shear stresses, the constitutive relations for the kth layer have the form

$$
\begin{Bmatrix} \sigma_x^{(k)} \\ \tau_{xz}^{(k)} \end{Bmatrix} = \begin{bmatrix} E_x^{(k)} & 0 \\ 0 & G_{xz}^{(k)} \end{bmatrix} \begin{Bmatrix} \varepsilon_x^{(k)} \\ \gamma_{xz}^{(k)} \end{Bmatrix}
\tag{8}
$$

where $E_x^{(k)}$ and $G_{xz}^{(k)}$ denote, respectively, the kth layer axial and transverse-shear moduli.

Note that the present zigzag function and associate kinematics give rise to the transverse shear strain of the form

$$
\gamma_{xz}^{(k)} = w_{,x} + \theta + \left[\left(\frac{G_{xz}^{(k)}}{h} \sum_{k=1}^{N} \frac{h^{(k)}}{G_{xz}^{(k)}} \right)^{-1} - 1 \right] \psi
\tag{9}
$$

In addition, the average quantities of Timoshenko theory also appear in this theory, i.e.,

$$
\theta \equiv \frac{1}{2h} \int_{-h}^{h} u_{x,z}^{(k)} dz \quad \text{and} \quad \gamma \equiv \frac{1}{2h} \int_{-h}^{h} \gamma_{xz}^{(k)} dz = w_{,x} + \theta
\tag{10}
$$

2.2. Virtual work principle

The Principle of Virtual Work (PVW) can be employed to derive the Euler–Lagrange equations of equilibrium and a set of consistent boundary conditions. Presently, starting with the two-dimensional elasticity theory and the corresponding form of the PVW, a one-dimensional variational statement is obtained and then used to develop several low-order beam elements. The two-dimensional PVW corresponding to the assumptions of RZT has the form

$$
\int_{x_a}^{x_b} \int_A [\delta\varepsilon_x^{(k)} \sigma_x^{(k)} + \delta\gamma_{xz}^{(k)} \tau_{xz}^{(k)}] dA dx - \int_{x_a}^{x_b} [\delta u_x^{(1)}(-h)p^b
$$
$$
+ \delta u_x^{(N)}(+h)p^t + \delta u_z^{(1)}(-h)q^b + \delta u_z^{(N)}(+h)q^t] dx
$$
$$
+ \int_A [T_{xa}\delta u_x^{(k)}(x_a, z) + T_{za}\delta w(x_a)] dA - \int_A [T_{xb}\delta u_x^{(k)}(x_b, z)
$$
$$
+ T_{zb}\delta w(x_b)] dA = 0
\tag{11}
$$

Substituting Eqs. (1) and (7) into Eq. (11) and integrating over the beam's cross-section, a one-dimensional form of the PVW is obtained (see Fig. 3)

$$
\int_{x_a}^{x_b} [N_x\delta u_{,x} + M_x\delta\theta_{,x} + V_x\delta(w_{,x} + \theta) + M_\phi\delta\psi_{,x}
$$
$$
+ V_\phi\delta\psi - p\delta u - q\delta w - m\delta\theta] dx
$$
$$
+ [\bar{N}_{xa}\delta u(x_a) + \bar{M}_{xa}\delta\theta(x_a) + \bar{V}_{xa}\delta w(x_a) + \bar{M}_{\phi a}\delta\psi(x_a)]
$$
$$
- [\bar{N}_{xb}\delta u(x_b) + \bar{M}_{xb}\delta\theta(x_b) + \bar{V}_{xb}\delta w(x_b) + \bar{M}_{\phi b}\delta\psi(x_b)] = 0
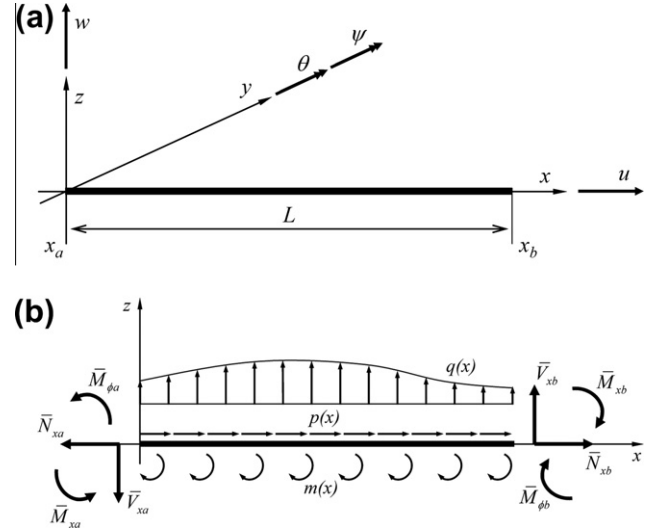\tag{12}
$$

Fig. 3. Kinematic variables, stress resultants, and applied loading for RZT beam: (a) kinematic variables and (b) applied loading.

where

$$
[N_x, M_x, M_\phi, V_x, V_\phi] \equiv \int_A [\sigma_x^{(k)}, z\sigma_x^{(k)}, \phi^{(k)}\sigma_x^{(k)}, \tau_{xz}^{(k)}, \beta^{(k)}\tau_{xz}^{(k)}] dA
\tag{13.1}
$$

$$
[\bar{N}_{x\alpha}, \bar{M}_{x\alpha}, \bar{M}_{\phi\alpha}, \bar{V}_{x\alpha}] \equiv \int_A [T_{x\alpha}, zT_{x\alpha}, \phi^{(k)}T_{x\alpha}, T_{z\alpha}] dA \ (\alpha = a, b)
\tag{13.2}
$$

are the reactive and applied stress resultants, and

$$
[p, q, m] = [p^b + p^t, q^b + q^t, h(p^t - p^b)]
\tag{14}
$$

are the combined distributed loads.

Integrating Eq. (13.1) while making use of Eqs. (2)–(8) results in the constitutive equations for the RZT beam

$$
\begin{Bmatrix} N_x \\ V_x \\ V_\phi \\ M_x \\ M_\phi \end{Bmatrix} = \begin{bmatrix} A_{11} & 0 & 0 & 0 & B_{12} & B_{13} \\ 0 & Q+\lambda & Q+\lambda & -\lambda & 0 & 0 \\ 0 & -\lambda & -\lambda & \lambda & 0 & 0 \\ B_{12} & 0 & 0 & 0 & D_{11} & D_{12} \\ B_{13} & 0 & 0 & 0 & D_{12} & D_{22} \end{bmatrix} \begin{Bmatrix} u_{,x} \\ w_{,x} \\ \theta \\ \psi \\ \theta_{,x} \\ \psi_{,x} \end{Bmatrix} \equiv \mathbf{D}\boldsymbol{\omega}
\tag{15}
$$

where the stiffness coefficients are defined as

$$
[A_{11}, B_{12}, D_{11}] \equiv \int_A E_x^{(k)} [1, z, z^2] dA, \quad [B_{13}, D_{12}, D_{22}] \equiv \int_A E_x^{(k)} \phi^{(k)} [1, z, \phi^{(k)}] dA,
$$
$$
[Q, \lambda] \equiv \int_A G_{xz}^{(k)} [(1 + \beta^{(k)})^2, (\beta^{(k)})^2] dA
\tag{16}
$$

Performing the variation by parts in Eq. (12) results in the Euler–Lagrange equilibrium equations

$$
\begin{aligned}
&N_{x,x} + p = 0 \\
&M_{x,x} - V_x + m = 0 \\
&V_{x,x} + q = 0 \\
&M_{\phi,x} - V_\phi = 0
\end{aligned}
\tag{17}
$$

and a set of consistent geometric (kinematic-variable) and kinetic (stress-resultant) boundary conditions at the beam ends, $x_\alpha \equiv (x_a, x_b)$, i.e.,

either $\quad u(x_\alpha) = \bar{u}_\alpha \quad$ or $\quad N_x(x_\alpha) = \bar{N}_{x\alpha}$

either $\quad \theta(x_\alpha) = \bar{\theta}_\alpha \quad$ or $\quad M_x(x_\alpha) = \bar{M}_{x\alpha}$

either $\quad w(x_\alpha) = \bar{w}_\alpha \quad$ or $\quad V_x(x_\alpha) = \bar{V}_{x\alpha}$ $\qquad$ (18)

either $\quad \psi(x_\alpha) = \bar{\psi}_\alpha \quad$ or $\quad M_\phi(x_\alpha) = \bar{M}_{\phi\alpha}$

where the bar-superscripted symbols denote the prescribed displacements and stress resultants. Whereas the first three equilibrium equations in Eq. (17) have the basic form of Timoshenko (or classical) theory, the fourth equation describes the higher-order moment-shear equilibrium associated with the cross-sectional distortions modelled by the zigzag function. In [14,15], the theory is assessed by way of the analytic (exact) solutions to Eqs. (15)–(18) for simply supported and cantilevered beams of various composite and sandwich laminates.

The one-dimensional variational statement, Eq. (12), can now be used to derive suitable beam elements. Since the strain quanti-ties in the variational statement do not exceed first spatial deriva-tives of the kinematic variables, C^0-continuous shape functions may be used to derive kinematically compatible beam elements. This aspect makes the use of RZT quite attractive for developing fi-nite elements. As can be observed, the form of Eq. (12) is analogous to that of Timoshenko theory; note that in this theory there are additional terms associated with the zigzag rotation variable, ψ, and its first derivative, $\psi_{,x}$.

3. Beam element formulation

To derive the beam-element stiffness matrix and forces vector corresponding to RZT, a suitable interpolation strategy has to be adopted and then used in the virtual work principle, Eq. (12). I n what follows, several viable interpolation schemes are examined.

3.1. Criteria for element interpolations; stiffness matrix and load vector

The standard formulation of Timoshenko beam elements, using the linear Lagrange polynomials for u, w and θ, and the full Gauss-ian quadrature necessary for obtaining exact integrals of the ele-ment matrices, always results in an element that tends to produce overly stiff solutions (with a near-zero curvature) for slen-der beams. This type of pathological behavior is commonly re-ferred to as *shear locking* [21]. Tessler and Dong (1981) identified the main modeling deficiency of the linear isoparametric element, recognizing that in the thin beam limit ($L/2h \to \infty$), the shear strain measure, relative to the curvature, must vanish in a limiting sense, i.e.,

$$\gamma = w_{,x} + \theta \to 0 \quad \text{or} \quad w_{,x} \to -\theta \qquad (19)$$

The implication is that the deflection $w(x)$ *needs to be approximated by a polynomial that is one degree higher than that used for $\theta(x)$, such that the above constraint condition can be achieved without any deleterious effects on the bending curvature.* This interpolation strategy was originally labelled *interdependent* to emphasize the interdependent nature of $w(x)$ and $\theta(x)$ approximations, and later the term *anisoparametric* interpolations was introduced to empha-size the different polynomial degrees used in interpolating the $w(x)$ and $\theta(x)$ variables, to contrast a commonly used term *isopara-metric interpolations*.

The *anisoparametric* interpolation strategy results in elements that have (i) an extra w-dof specified at a node that has no other dof's (Fig. 4a), and (ii) the transverse shear strain and force that are described by a polynomial one degree higher than the polyno-mial which interpolates the bending strain and moment. A simple resolution is to develop the corresponding *constrained* elements that have the standard, isoparametric-like nodal patterns
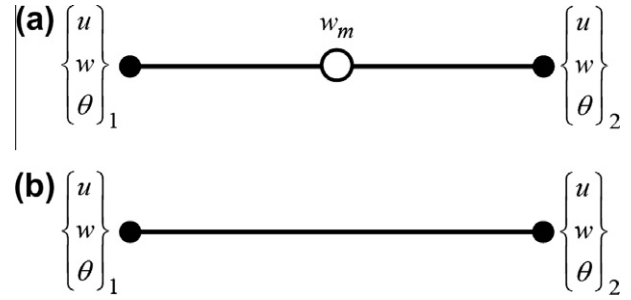

Fig. 4. Nodal configurations for three- and two-node *anisoparametric* elements based on Timoshenko theory [24]: (a) anisoparametric element and (b) constrained anisoparametric element.

(Fig. 4b). This is accomplished by reducing the polynomial degree of the shear strain measure, γ, (or, equivalently, the shear force V_x) by one order, resulting in a coupled deflection interpolation in which the rotational dof's contribute to the deflection only in the interior part of the element.

3.2. Three-node, nine-dof anisoparametric element

Employing the *anisoparametric* (*interdependent*) interpolation strategy, the *lowest-order RZT element* can now be formulated by interpolating the kinematic variables as follows

$$\mathbf{u} = \begin{Bmatrix} u \\ w \\ \theta \\ \psi \end{Bmatrix} = \mathbf{N}\mathbf{u^e} \qquad (20)$$

where $\mathbf{N}$ is a matrix containing the shape functions, and $\mathbf{u^e}$ is the vector of nodal dof's; the $\mathbf{N}$ and $\mathbf{u^e}$ are defined as

$$\mathbf{N} = \begin{bmatrix} N_1^L & 0 & 0 & 0 & 0 & N_2^L & 0 & 0 & 0 \\ 0 & N_1^Q & 0 & 0 & N_m^Q & 0 & N_2^Q & 0 & 0 \\ 0 & 0 & N_1^L & 0 & 0 & 0 & 0 & N_2^L & 0 \\ 0 & 0 & 0 & N_1^L & 0 & 0 & 0 & 0 & N_2^L \end{bmatrix} \qquad (21.1)$$

$$\mathbf{u^e} = [\, u_1 \quad w_1 \quad \theta_1 \quad \psi_1 \quad w_m \quad u_2 \quad w_2 \quad \theta_2 \quad \psi_2 \,]^T \qquad (21.2)$$

and

$$[N_1^L, N_2^L] = \left[\frac{1}{2}(1-\xi), \frac{1}{2}(1+\xi) \right],$$

$$[N_1^Q, N_m^Q, N_2^Q] = \left[\frac{1}{2}\xi(\xi-1), (1-\xi^2), \frac{1}{2}\xi(\xi+1) \right] \qquad (21.3)$$

where $\xi \equiv 2x/L^e - 1 \in [-1, 1]$ is a non-dimensional axial coordinate, with $x \in [0, L^e]$ and L^e denoting the element length; the $N_i^L(\xi)(i = 1, 2)$ and $N_j^Q(\xi)(j = 1, m, 2)$ are respectively the standard linear and quadratic Lagrange polynomials. For the nodal pattern of this element refer to Fig. 5a.

3.3. Two-node, eight-dof constrained anisoparametric elements

In the constitutive relations of RZT, Eq. (15), the transverse shear force is a function of the two strain measures,

$$\gamma(x) = w_{,x}(x) + \theta(x) \quad \text{and} \quad \eta(x) = w_{,x}(x) + \theta(x) - \psi(x) \qquad (22)$$

and, in terms of these strain measures, $V_x(x)$ can be expressed as

$$V_x(x) = Q\gamma(x) + \lambda\eta(x) \qquad (23.1)$$

or, alternatively, $V_x(x)$ can be expressed in terms of the $\gamma(x)$ and $\psi(x)$ quantities
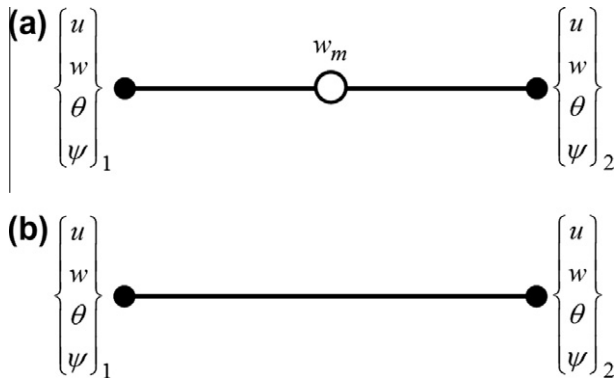
Fig. 5. Nodal configurations for three- and two-node *anisoparametric* elements based on Refined Zigzag Theory for beams: (a) anisoparametric element and (b) constrained anisoparametric element.

$$V_x(x) = (Q + \lambda)[\gamma(x) + r\psi(x)] \tag{23.2}$$

where $r \in [-1, 0]$ is a dimensionless transverse-shear material parameter given by

$$r \equiv -\frac{\lambda}{Q + \lambda} = \frac{\int_A \beta^{(k)} G_{xz}^{(k)} dA}{\int_A G_{xz}^{(k)} dA} \tag{24}$$

The extreme values of this material parameter are: (a) $r = 0$ for homogeneous cross-sections (when $\beta^{(k)} = 0$), and (b) $r \to -1$ for highly heterogeneous cross-sections, such as in soft-core sandwich laminates (refer to the numerical studies in Section 5).

In Eq. (23) the transverse shear force, $V_x(x)$, has the proper linear interpolation since $\gamma(x)$, $\eta(x)$, and $\psi(x)$ are linear functions of the x coordinate. Both $\gamma(x)$ and $\eta(x)$ include $w_{,x}(x)$ (deflection slope) which is also linear. Intuitively, with reference to Eq. (23.1), the 'optimal' constraining strategy for condensing out the w_m dof would be to reduce the $V_x(x)$ distribution from a linear to a constant. This constraint scheme would retain the linear character for both $\gamma(x)$ and $\eta(x)$ while making $w_m = w_m(w_i, \theta_i, \psi_i, r, L^e)$ (dependent on the w_i, θ_i and ψ_i ($i = 1, 2$) dof's at the two end nodes, the material parameter, r, and the element length, L^e). Alternatively, the polynomial degree reduction of either $\gamma(x)$ or $\eta(x)$ can be implemented leading to $w_m = w_m(w_i, \theta_i, L^e)$ in the first case, and $w_m = w_m(w_i, \theta_i, \psi_i, L^e)$ in the second, with the latter scheme ($\eta = const.$) appearing to be preferable over the former ($\gamma = const.$).

The expression for w_m that encompasses all three constraint strategies just described has the form

$$w_m = \frac{w_1 + w_2}{2} + \frac{L^e}{8}[(\theta_2 + c\psi_2) - (\theta_1 + c\psi_1)] \tag{25}$$

where (i) $c = r$ if $V_x = const.$, (ii) $c = -1$ if $\eta = const.$, and (iii) $c = 0$ if $\gamma = const.$

The constrained deflection that also encompasses all three constraint cases is given by the hierarchical form

$$w(x) = \frac{1}{2}(1 - \xi)w_1 + \frac{1}{2}(1 + \xi)w_2 + \alpha \frac{L^e}{8}(1 - \xi^2)[(\theta_2 + c\psi_2) - (\theta_1 + c\psi_1)] \tag{26}$$

where the leading term is the standard linear Lagrange interpolation in terms of the w_i ($i = 1, 2$) dof's, and the higher-order term is a bubble function which vanishes at the two end nodes of the beam element. The tracer α, which equals 1 in this formulation, can be set to 0 to exclude the bubble-function term in order to obtain the linear *isoparametric* interpolation.

The shape function matrix and the vector of nodal dof's for the *constrained* elements, including the linear element, has the form (refer to Fig. 5b for the nodal pattern of these elements)

$$\mathbf{N} = \begin{bmatrix} N_1^L & 0 & 0 & 0 & N_2^L & 0 & 0 & 0 \\ 0 & N_1^L & -\alpha \frac{L^e}{8} N_m^Q & -\alpha c \frac{L^e}{8} N_m^Q & 0 & N_2^L & \alpha \frac{L^e}{8} N_m^Q & \alpha c \frac{L^e}{8} N_m^Q \\ 0 & 0 & N_1^L & 0 & 0 & 0 & N_2^L & 0 \\ 0 & 0 & 0 & N_1^L & 0 & 0 & 0 & N_2^L \end{bmatrix} \tag{27}$$

$$\mathbf{u}^e = \begin{bmatrix} u_1 & w_1 & \theta_1 & \psi_1 & u_2 & w_2 & \theta_2 & \psi_2 \end{bmatrix}^T$$

3.4. Element stiffness matrix and load vector

Substituting Eq. (20) into Eq. (15) and then into Eq. (12), and after some straightforward operations, the element-level equilibrium equations take on the matrix form

$$\mathbf{K}^e \mathbf{u}^e = \mathbf{f}^e \tag{28}$$

The stiffness matrix may be calculated as follows

$$\mathbf{K}^e = \int_0^{L_e} \mathbf{B}^{eT} \mathbf{D} \mathbf{B}^e dx \tag{28a}$$

where $\mathbf{B}^e$ is the element strain–displacement matrix containing the derivatives of the shape functions with respect to the x-coordinate, and $\mathbf{D}$ is the beam constitutive matrix defined in Eqs. (15) and (16). The $\mathbf{B}^e$ matrices corresponding to the three-node *anisoparametric* and two-node *constrained* elements are summarized in Appendix A.

For the case of distributed loading due to p, q, and m, Eq. (14), the element consistent load vector, $\mathbf{f}^e$, is defined as

$$\mathbf{f}^e = \int_0^{L_e} \widehat{\mathbf{N}}^T \mathbf{q} dx \tag{28b}$$

where $\widehat{\mathbf{N}}$ is composed by the first three rows of shape-function matrix, $\mathbf{N}$ (Eqs. (21.1) and (27)), and $\mathbf{q} \equiv [p(x), q(x), m(x)]^T$.

4. Example problems and numerical results

In this section analytic and finite element results are presented, first highlighting the capability of RZT to model laminated composite and sandwich laminates, and then focusing on the predictive capabilities of the RZT-based beam elements.

4.1. Problem description

Simply supported and cantilevered three-layered beams are considered, having various laminations and material compositions through the depth. Unless specified otherwise, the beam has a rectangular cross-section of width, $b = 4$ cm, depth $2h = 4$ cm, and span $L = 20$ cm. The mechanical material properties are summarized in Table 1. In Table 2 are listed the laminate ply-thickness distributions, material stacking sequences, and magnitudes of the applied loadings. Material "f" has a variable Young's modulus ranging from 7.3×10^{-4} to 73.0 GPa, and a transverse shear modulus that is calculated by using a Poisson ratio of 0.25. The material layer thicknesses are denoted as $2h^{(1)}$, $2h^{(2)}$, and $2h^{(3)}$, where the first layer starts at $z = -h$ (refer to Fig. 2).

The simply supported beam is subjected to the transverse pressure loading given by the sine function $q(x) = q_0 \sin(\pi x/L)$, with the geometric boundary conditions defined as (see Fig. 6a)

$$w = 0 \text{ at } x = 0, L \tag{29}$$

The cantilevered beam is subjected to three distinct loading conditions which include a tip transverse shear force, F, applied at $x = L$ (Fig. 6b), a uniform pressure applied along the top surface (Fig. 6c), and a linearly distributed pressure applied along the top

Table 1
Material mechanical properties.

Material type	Young's modulus $E_x^{(k)}$ (GPa)	Shear modulus $G_{xz}^{(k)}$ (GPa)
a	73.0	29.2
b	21.9	8.76
c	3.65	1.46
d	0.73	0.292
e	0.073	0.029
f	Ranging from 7.3×10^{-4} to 73.0	$E_x^{(k)}/2.5$

Table 2
Laminate stacking sequences and applied loading. (Note: the first layer is the bottom layer.)

Laminate designation	Normalized layer thickness $2h^{(i)}/2h$	Materials	Applied loads	
			q_0 (N/m)	F (N)
A	(0.10/0.80/0.10)	(a/e/b)	3×10^6	2×10^3
C	(0.33/0.33/0.33)	(d/a/c)	2×10^{-3}	–
D	(0.33/0.33/0.33)	(a/f/a)	1.5×10^7	–

surface (Fig. 6d). The geometric boundary conditions for the canti-levered beam are

$$u = w = \theta = \psi = 0 \text{ at } x = 0 \qquad (30)$$

Note that the transverse shear strain at the clamped end ($x = 0$) is simply $\gamma_{xz} = w_{,x}$, which is a non-vanishing quantity for this theory (see the discussion in [15] on the clamped-end anomaly engen-dered by other zigzag theories).

4.2. Review of RZT predictive capabilities

A cantilevered beam under a transverse shear force, F, applied at the tip ($x = L$) is analyzed using the laminate stacking sequence A (see Table 2). The RZT analytic solutions, labeled "RZT", are depicted in Figs. 7–11. In addition, for comparison purposes the following solutions are also shown in the figures: (i) a reference solution, labeled "NASTRAN", using a high-fidelity, two-dimensional, plane-stress FEM model obtained with MSC/NASTRAN®
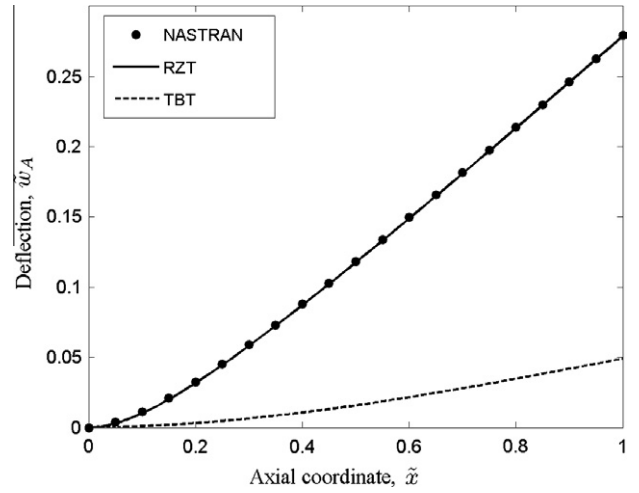

Fig. 7. Normalized deflection of a cantilevered beam under a tip shear force (laminate A, $\rho = 5$).
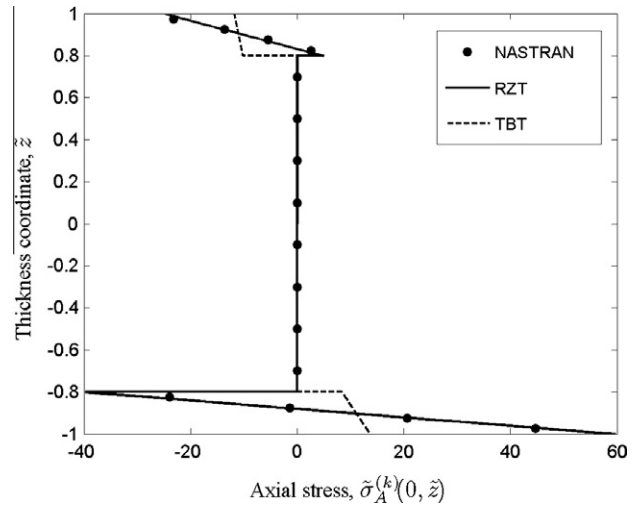

Fig. 8. Normalized axial stress at the clamped end of a cantilevered beam under a tip shear force (laminate A, $\rho = 5$).
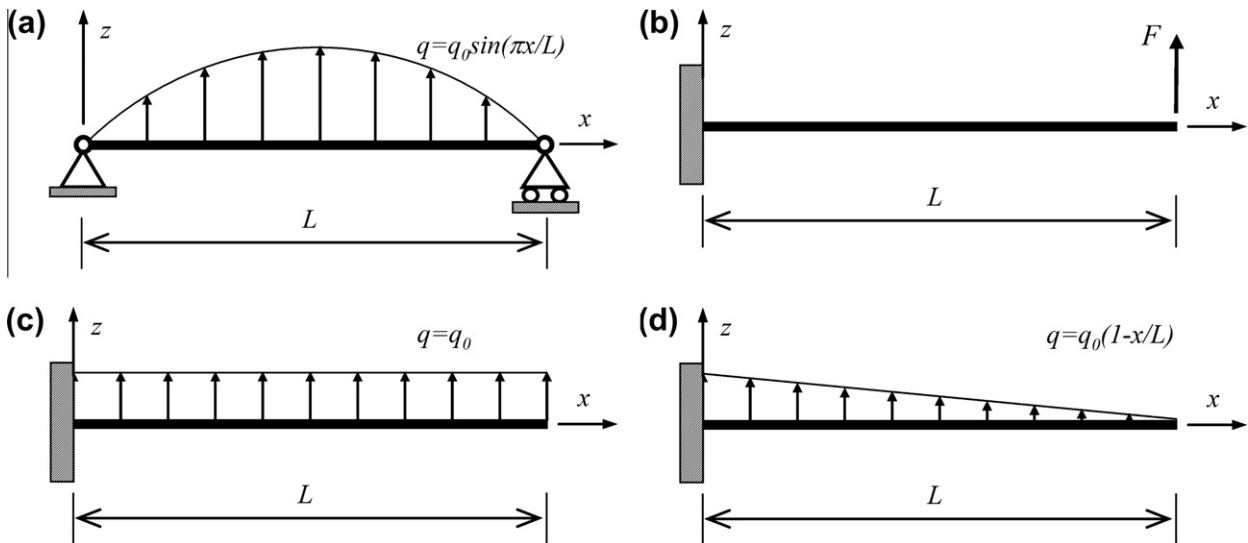

Fig. 6. Geometry, boundary conditions, and applied loading for the four example problems: (a) simply supported beam under sinusoidal pressure, (b) cantilevered beam under tip shear force, (c) cantilevered beam under uniform pressure and (d) cantilevered beam under linear pressure.
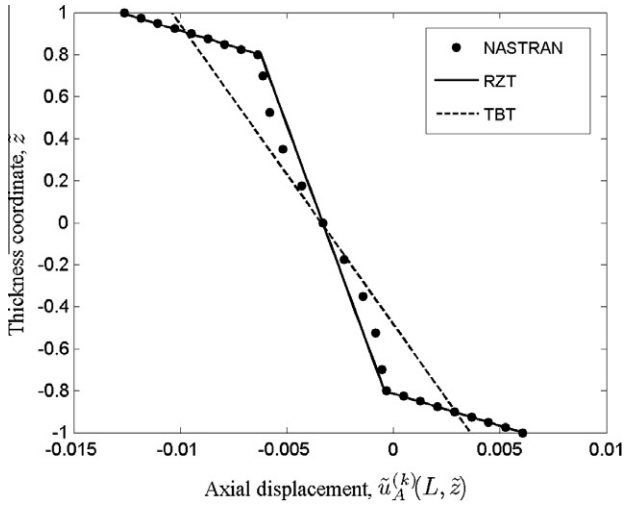
Fig. 9. Normalized axial displacement at the free end of a cantilevered beam under a tip shear force (laminate A, $\rho = 5$).
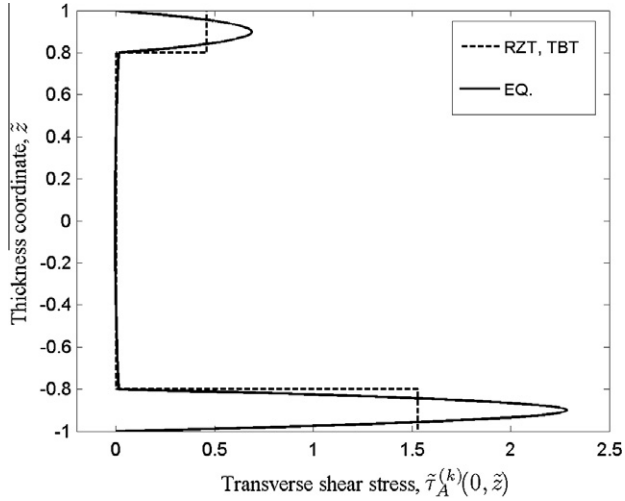

Fig. 10. Normalized transverse shear stress at the clamped end of a cantilevered beam under a tip shear force (laminate A, $\rho = 5$).
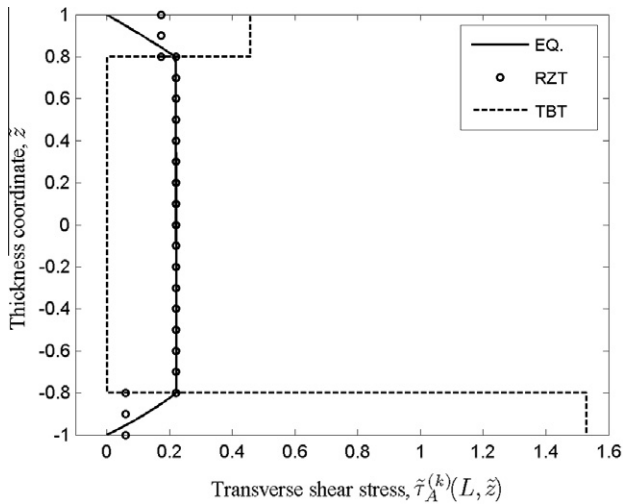

Fig. 11. Normalized transverse shear stress at the free end of a cantilevered beam under a tip shear force (laminate A, $\rho = 5$).

Table 3
Element designation, kinematic interpolation, and nodal configuration.

Element type	Deflection interpolation	Constraint imposed	No. of nodes (dof's) (Figs. 4,5)
Ω_L: Linear isoparametric	Eq. (26): $\alpha = 0$	None	2 (8)
Ω_0: Anisoparametric	Eqs. (20), (21)	None	3 (9)
Ω_γ: Constrained anisoparametric	Eq. (26): $\alpha = 1$, $c = 0$	$\gamma = $ const.	2 (8)
Ω_η: Constrained anisoparametric	Eq. (26): $\alpha = 1$, $c = -1$	$\eta = $ const.	2 (8)
Ω_V: Constrained anisoparametric	Eq. (26): $\alpha = 1$, $c = r$	$V_x = $ const.	2 (8)

[14]; (ii) an analytic solution using Timoshenko Beam Theory (shear correction factor $k^2 = 5/6$), labeled "TBT", and (iii) a transverse shear-stress solution, labeled "EQ.", which is obtained by integrating the elasticity-theory equilibrium equation $\sigma_{x,x}^{(k)} + \tau_{xz,z}^{(k)} = 0$, where $\sigma_x^{(k)}$ represents the axial stress computed by RZT.

In the figures, the special coordinates and response quantities are normalized as follows

$$(\tilde{x}, \tilde{z}) \equiv (x/L, z/h),$$
$$\left(\tilde{u}_A^{(k)}, \tilde{w}_A\right) \equiv \frac{D_{11}}{10FL^3}(u_x^{(k)}, w), \quad \left(\tilde{\sigma}_A^{(k)}, \tilde{\tau}_A^{(k)}\right) \equiv \frac{A}{F\rho}\left(\sigma_x^{(k)}, \tau_{xz}^{(k)}\right) \quad (31)$$

where $\rho = L/2h$ represents the beam span-to-span ratio. The RZT analytic solutions are in close agreement with the NASTRAN predictions and are also considerably more accurate than those of Timoshenko theory: TBT underestimates the maximum deflection by over 80% (Fig. 7) and the maximum axial stress by over 75% (Fig. 8). Fig. 9 reveals that RZT provides a highly accurate assess-ment of the axial displacement through the depth of the beam, manifesting in a zigzag-like distribution. Fig. 10 depicts the trans-verse shear stress at the clamped end where both TBT and RZT pro-vide relatively accurate piecewise-constant approximations of the stress. However, at the tip of the beam (Fig. 11) only RZT retains the desired degree of accuracy – the transverse shear stress com-puted by RZT has a correct variation along the beam's span, whereas TBT is limited to a non-varying (constant) solution and, as evi-denced from the reference solution, its solution is erroneous.
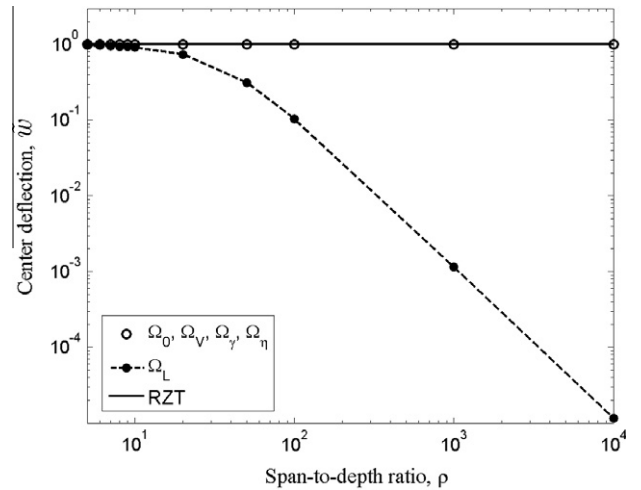

Fig. 12. Normalized center deflection, $\tilde{w}(L/2)$, versus span-to-depth ratio, ρ, for a simply supported beam under sinusoidal pressure (laminate C; $n^e = 50$ discretization).

Table 4
Simply supported beam, laminate D, $\rho = 5$. Normalized center deflection, $\tilde{w}(L/2)$, obtained with Ω_0, Ω_V, Ω_η, and Ω_γ element discretizations, for different number of elements, n^e, and material parameter, r.

Stacking sequence properties		Core-to-face Young's modulus ratio, $E_x^{(2)}/E_x^{(1)}$ (refer to Tables 1 and 2)							
		10^{-5}	10^{-4}	10^{-3}	10^{-2}	10^{-1}	9×10^{-1}	9.99×10^{-1}	9.9999×10^{-1}
		Material parameter, r							
		-1.000	-9.996×10^{-1}	-9.955×10^{-1}	-9.561×10^{-1}	-6.429×10^{-1}	-2.463×10^{-3}	-2.224×10^{-7}	-2.22×10^{-11}
n^e	Elem.	Normalized center deflection $\bar{w}$							
6	Ω_0, Ω_V	0.977	0.978	0.981	0.990	0.985	0.979	0.979	0.979
	Ω_η	0.977	0.978	0.981	0.990	0.984	0.971	0.972	0.972
	Ω_γ	0.483	0.489	0.540	0.784	0.970	0.979	0.979	0.979
10	Ω_0, Ω_V	0.992	0.992	0.993	0.996	0.995	0.993	0.992	0.992
	Ω_η	0.992	0.992	0.993	0.996	0.994	0.986	0.985	0.985
	Ω_γ	0.714	0.719	0.759	0.908	0.989	0.993	0.992	0.992
50	Ω_0, Ω_V	1.000	1.000	1.000	1.000	1.000	1.000	1.000	1.000
	Ω_η	1.000	1.000	1.000	1.000	1.000	0.999	0.992	0.992
	Ω_γ	0.984	0.984	0.987	0.996	1.000	1.000	1.000	1.000

Table 5
Cantilevered beam, laminate A, $\rho = 5$. Normalized deflection, $w_{\Omega_V}/w_{\Omega_0}$, at various locations for one and two element discretizations and three loading conditions.

n^e	1			2				
Points along the beam	–	A	B	–	A	B	C	D
Tip load	–	1.000	1.000	–	1.000	1.000	1.000	1.000
Uniform load	–	0.987	1.000	–	0.995	1.000	0.999	1.000
Linear load	–	0.974	1.000	–	0.987	1.000	0.999	1.000

4.3. Beam element results

To facilitate the discussion of the beam finite element results, Table 3 summarizes the element designation and their associate kinematic interpolations and nodal configurations. Subsequently, the label "A" is used to denote an analytic solution obtained by RZT [14,15], whereas "FEM" denotes a finite element solution using one of the present beam elements, and n^e indicates the number of elements used in a uniform discretization of a beam. Thus, in the present convergence studies the following response quantities are examined: (a) deflection, $\tilde{w} \equiv w_{FEM}/w_A$, computed at the center ($x = L/2$) of simply supported beams and at the tip ($x = L$) of cantilevered beams; (b) axial displacement, $\tilde{u} \equiv u_{FEM}/u_A(L, -h)$; (c) axial stress, $\tilde{\sigma} \equiv \sigma_{FEM}/\sigma_A(L^e/2, -h)$, and (d) transverse shear stress, $\tilde{\tau} \equiv \tau_{FEM}/\tau_A(L^e/2, -h)$. The computed values of the RZT analytic solutions [w_A, u_A, σ_A, and τ_A] are summarized in Appendix B.

Initially, the element performance is examined over a range of span-to-depth ratios, $\rho = L/2h$, with the focus on slender beams for ρ is relatively large. Herein the simply supported beam in Fig. 6a (laminate C) is analyzed using the $n^e = 50$ discretization. In Fig. 12, the maximum (center) deflection, $\tilde{w}$, is plotted versus ρ, where the finite element solutions for the Ω_L, Ω_0 and Ω_V elements are represented. The results obtained with the Ω_γ and Ω_η elements are practically identical to those of the Ω_V element. The results show that the RZT-based linear isoparametric element, Ω_L, suffers from shear locking – the behavior that manifests itself with progressively stiffer response as the beam becomes more slender. In contrast, the four anisoparametric elements do not exhibit any deterioration for slender beams.

The following numerical study is focused on demonstrating the differences in the predictive capabilities between the four anisoparametric elements considered herein, by examining their performance over a wide range of material heterogeneity and anisotropy. In Table 4, the maximum deflection results for a deep simply supported beam (laminate D, $\rho = 5$) are compared for the four anisoparametric elements, where the laminate material properties are varied from highly heterogeneous ($r \rightarrow -1$) to nearly homogeneous ($r \rightarrow 0$).[1] For the finest discretization, $n_e = 50$, the four anisoparametric elements produce comparably accurate results. The largest discrepancies are manifested for the $n_e = 6$ mesh – the coarsest mesh in this study. At this level of discretization and for $r \rightarrow -1$ (highly heterogeneous cross-sections), the Ω_0, Ω_V and Ω_η elements produce nearly identical results of high accuracy, where the errors do not exceed 3%; whereas the Ω_γ element solution (for $n_e = 6$) underestimates the deflection by about 50%. The Ω_γ results, however, tend to improve as $r \rightarrow 0$ (nearly homogeneous cross-sections). The results for the Ω_0 and Ω_V are consistently identical at the end-nodes. The Ω_η element predictions are only slightly less accurate than those of the Ω_0 and Ω_V elements. Of the three versions of con-strained elements the Ω_V element is the best performer. For this rea-son subsequent numerical results will focus on the relative accuracy of the Ω_V and Ω_0 elements.

Since both Ω_V and Ω_0 predict identical displacements at the end nodes, it is worth to examine if there exist any discrepancies

---

[1] Recently, in [19,20], the authors proposed the *Homogeneous Limit Modelling* (HLM) strategy to model the response of homogeneous beams accurately. The HLM methodology takes full advantage of the RZT's zigzag kinematics even for homogeneous beams: the RZT does not degenerate to Timoshenko theory and requires no shear correction factors. The approach yields superior predictions for all of the response quantities including the strains and stresses, producing highly accurate parabolic shear stress and cubic axial stress distributions through-the-thickness in deep homogeneous beams. The deflection predictions with and without the use of HLM, however, do not differ substantially. It is noted that in generating the results in Table 4 for $r \rightarrow 0$, the HLM was not employed.

between the results within the element span produced by these elements. In Table 5, maximum deflection results are compared for the problem of a cantilevered beam (laminate A) subjected to various transverse loads, for one- and two-element discretizations. It is seen that slightly different results are obtained within an element when the beam is subjected to a distributed loading. For example, for ne = 2, the differences are less than 2%. All other response quan-tities, including the kinematic variables [u(x), h(x), w(x)] and the ax-ial strain and stress [eðxkÞ; rðxkÞ] are predicted identically by the two types of elements. This is because u(x), h(x), and w(x) are interpo-lated by the same linear interpolations. At the element centers, the axial and transverse-shear strain and stress predictions by XV and X0 correspond identically. Clearly, the XV element represents the desirable compromise between the nodal simplicity, accuracy, and computational efficiency. Furthermore, the XV element, based on the constant shear-force constraint, ensures comparable accu-racy even when the global, beam-level distribution is non constant, in the case of a distributed shear loading.

Convergence studies examining displacement and stress predic-tionsg., by the various anisoparametric elements for the cantilevered beam under a tip shear force are shown in Figs. 13–15, and for the simply supported beam under sinusoidal pressure (laminate A), in
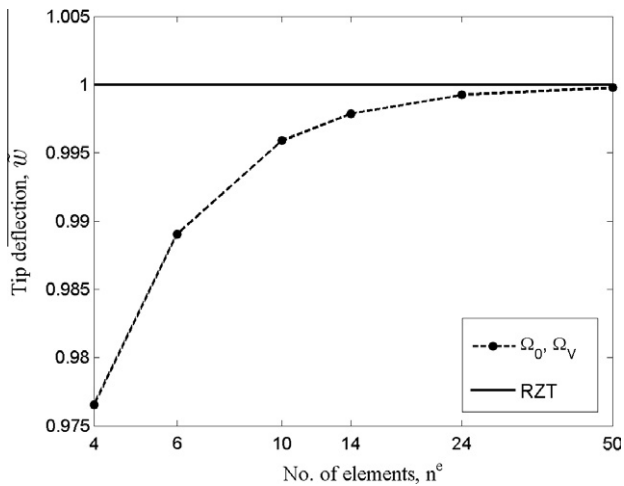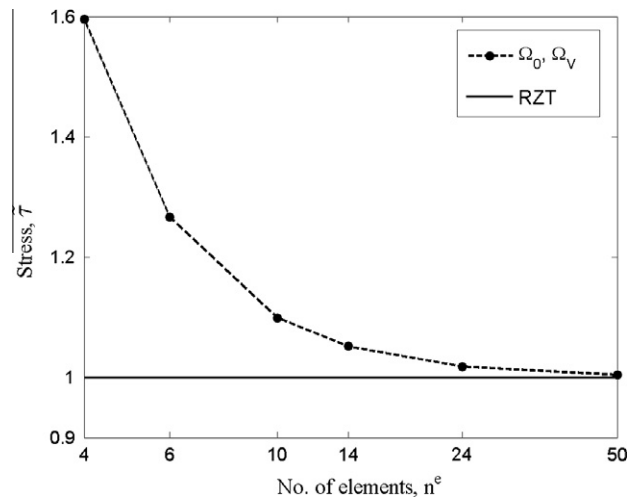

Fig. 15. Convergence of normalized transverse shear stress $\bar{\tau}(L^e/2, -h)$ for a cantilevered beam under a tip shear force using Ω_0 and Ω_V element discretizations (laminate A, $\rho = 5$).

Fig. 13. Convergence of normalized tip deflection, $\bar{w}(L)$, for a cantilevered beam under a tip shear force using Ω_0 and Ω_V element discretizations (laminate A, $\rho = 5$).
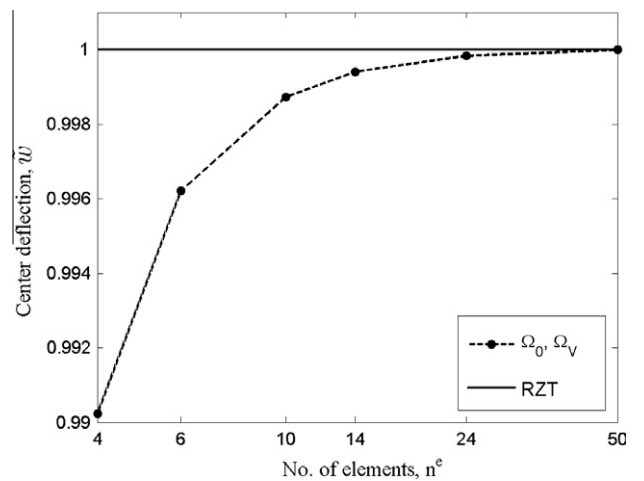

Fig. 16. Convergence of normalized center deflection, $\bar{w}(L/2)$, for a simply supported beam under sinusoidal pressure using Ω_0 and Ω_V element discretizations (laminate A, $\rho = 5$).
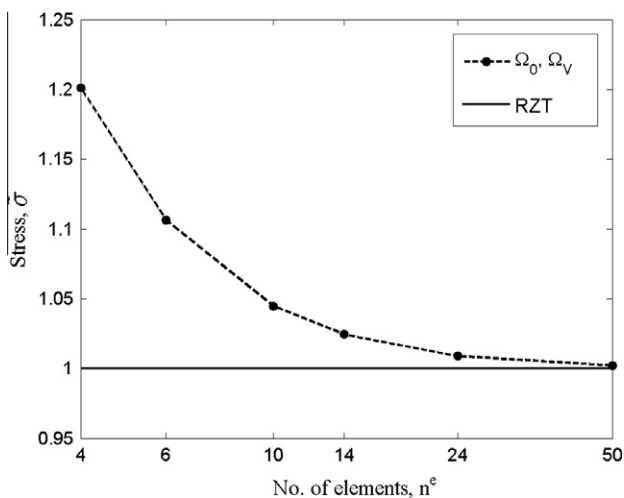

Fig. 14. Convergence of normalized axial stress $\bar{\sigma}(L^e/2, -h)$ for a cantilevered beam under a tip shear force using Ω_0 and Ω_V element discretizations (laminate A, $\rho = 5$).
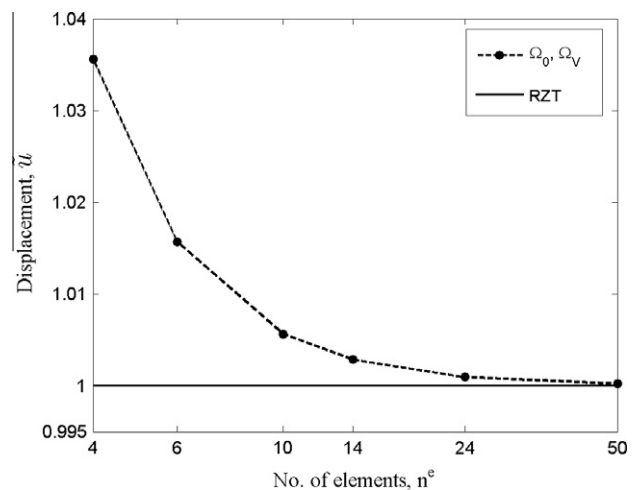

Fig. 17. Convergence of normalized axial displacement, $\bar{u}(L, -h)$, for a simply supported beam under sinusoidal pressure using Ω_0 and Ω_V element discretizations (laminate A, $\rho = 5$).
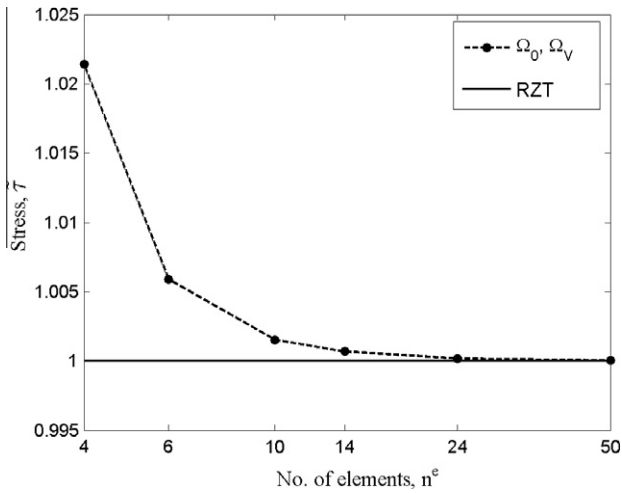
Fig. 18. Convergence of normalized transverse shear stress, $\bar{\tau}(L^e/2, -h)$, for a simply supported beam under sinusoidal pressure using Ω_0 and Ω_V element discretizations (laminate A, $\rho = 5$).

Figs. 16–18. Figs. 13 and 16 depict rapid convergence of the maximum deflection where even a coarse discretization ($n_e = 4$) leads to errors not exceeding 2.5%. Note that for the cantilevered beam problem, the analytic solutions for the kinematic unknowns u, w, θ, and ψ in the framework of RZT involve both polynomial and hyperbolic functions [15] – hence the need for a relatively fine discretization to achieve displacement convergence. The convergence of the axial displacement, Fig. 17, is also rapid. As evidenced from Figs. 14, 15 and 18, to achieve accurate stresses, finer discretizations are required. A slightly slower convergence is observed for the transverse shear stress, Fig. 15, where for the mesh $n^e = 15$ the error in the transverse shear stress is under 5%. These results further demonstrate that the Ω_V and Ω_0 element solutions produce identical predictions for the kinematic dof's at the element end nodes as well as the identical strains and stresses at the element centers.

5. Conclusions

In this paper, simple and efficient three- and two-node beam elements were developed which include the effects of the axial stretching, transverse shear deformation, and zigzag kinematics. The underlying structural theory is the Refined Zigzag Theory (RZT) for multilayered composite and sandwich beams recently developed by the authors. For planar deformations, four kinematic variables – one more than in Timoshenko theory – are required within RZT. The additional kinematic variable, the zigzag rotation, ensures a zigzag-like axial displacement and piecewise-constant rotations closely resembling solutions of elasticity theory for laminated composite structures. The theory enables a more accurate representation of all displacement, stress-resultant, strain and stress quantities, and unlike Timoshenko theory there is no reliance on shear correction factors to yield accurate results.

The *anisoparametric* (aka *interdependent*), C^0-continuous interpolations were employed for the kinematic variables of the theory to obtain a three-node element. This interpolation strategy, which involves independent assumptions of a quadratic deflection and linear interpolations for the axial displacement, bending rotation, and zigzag rotation, ensures free of shear locking performance for the entire range of moderately thick to very slender beams.

By imposing three types of continuous shear constraints – two on the distribution of the transverse shear-strain measures and one on the distribution of the transverse shear force – three constrained elements were generated, each having the desired

two-node configuration. Stiffness and consistent load vectors were formulated by Gaussian quadrature using formulas for exact integration. For comparison purposes, a fully integrated, two-node isoparametric linear element was also formulated and examined in the studies of shear locking. This latter element was shown to exhibit severe stiffening due to shear locking.

The new anisoparametric RZT-based elements demonstrated excellent modelling capabilities and suffered no shear locking effects. The constrained anisoparametric elements produced comparable accuracy of the unconstrained element, with the element derived on the basis of a constant shear-force constraint demonstrating the best overall performance of the three constrained elements. An important aspect of this two-node element is that it is a true constant-stress beam element, with all of its classical stress resultants being constant along the element length, thus enabling optimal stress evaluation at the element center.

Appendix A

The strain–displacement $\mathbf{B}^e$ matrix for the three-node, nine-dof *anisoparametric* element is given by

$$\mathbf{B^e} = \frac{1}{L_e} \begin{bmatrix} N^L_{1,\xi} & 0 & 0 & 0 & 0 & N^L_{2,\xi} & 0 & 0 & 0 \\ 0 & N^Q_{1,\xi} & 0 & 0 & N^Q_{m,\xi} & 0 & N^Q_{2,\xi} & 0 & 0 \\ 0 & 0 & L_e N^L_1 & 0 & 0 & 0 & 0 & L_e N^L_2 & 0 \\ 0 & 0 & 0 & L_e N^L_1 & 0 & 0 & 0 & 0 & L_e N^L_2 \\ 0 & 0 & N^L_{1,\xi} & 0 & 0 & 0 & 0 & N^L_{2,\xi} & 0 \\ 0 & 0 & 0 & N^L_{1,\xi} & 0 & 0 & 0 & 0 & N^L_{2,\xi} \end{bmatrix}$$

$$(A.1)$$

Table B1
Simply supported beam, laminate C. Analytic center deflection, $w_A(L/2)$, obtained with Refined Zigzag Theory for different span-to-thickness ratios.

Laminate thickness 2 h (mm)	Span-to-thickness ratio, ρ	Center deflection $w_A(L/2)$ (mm)
40.000	5	1.319×10^{-9}
33.333	6	2.265×10^{-9}
28.571	7	3.584×10^{-9}
25.000	8	5.338×10^{-9}
22.222	9	7.588×10^{-9}
20.000	10	1.024×10^{-8}
10.000	20	8.286×10^{-8}
4.000	50	1.293×10^{-6}
2.000	10^2	1.034×10^{-5}
0.200	10^3	10.0×10^{-3}
0.020	10^4	10.340

Table B2
Analytic results using Refined Zigzag Theory for laminate A, $\rho = 5$.

Problem	Deflection (mm)	Axial displacement $u_A(L, -h)$ (mm)	Stresses at $z = -h$		
			x/L	σ_A (Mpa)	τ_A (Mpa)
Simply supported beam under sinusoidal pressure	$w_A(L/2)$	−0.373	1/8	−163.686	4.428
	9.759		1/12	−110.706	4.629
			1/20	−66.912	4.731
			1/28	−47.892	4.761
			1/48	−27.975	4.782
			1/100	−13.434	4.788
Cantilevered beam under tip shear force	$w_A(L)$	0.199	1/8	161.205	3.128
	9.014		1/12	207.338	4.488
			1/20	258.950	6.045
			1/28	286.350	6.883
			1/48	319.025	7.885
			1/100	345.800	8.713

Table B3
Simply supported beam, laminate D, $\rho = 5$. Analytic center deflection $w_A(L/2)$ obtained with Refined Zigzag Theory for different core-to-face Young's modulus ratio.

Core to face Young's modulus ratio, $E_x^{(2)}/E_x^{(1)}$ (Tables 1 and 2)	Material parameter, r	Center deflection, $w_A(L/2)$ (mm)
10^{-5}	−1.000	8.603
10^{-4}	-9.996×10^{-1}	8.437
10^{-3}	-9.955×10^{-1}	7.094
10^{-2}	-9.561×10^{-1}	3.030
10^{-1}	-6.429×10^{-1}	1.000
9×10^{-1}	-2.463×10^{-3}	0.696
9.99×10^{-1}	-2.224×10^{-7}	0.690
9.9999×10^{-1}	-2.222×10^{-11}	0.690

whereas for the two-node, eight-dof *constrained anisoparametric* elements, $\mathbf{B^e}$ has the form

$$\mathbf{B^e} = \frac{1}{L_e}\begin{bmatrix} N_{1,\xi}^L & 0 & 0 & 0 & N_{2,\xi}^L & 0 & 0 & 0 \\ 0 & N_{1,\xi}^L & -\alpha\frac{L^e}{8}N_{m,\xi}^Q & -\alpha c\frac{L^e}{8}N_{m,\xi}^Q & 0 & N_{2,\xi}^L & \alpha\frac{L^e}{8}N_{m,\xi}^Q & \alpha c\frac{L^e}{8}N_{m,\xi}^Q \\ 0 & 0 & L_e N_1^L & 0 & 0 & 0 & L_e N_2^L & 0 \\ 0 & 0 & 0 & L_e N_1^L & 0 & 0 & 0 & L_e N_2^L \\ 0 & 0 & N_{1,\xi}^L & 0 & 0 & 0 & N_{2,\xi}^L & 0 \\ 0 & 0 & 0 & N_{1,\xi}^L & 0 & 0 & 0 & N_{2,\xi}^L \end{bmatrix}$$
(A.2)

Appendix B

The results summarized in the following tables correspond to the analytic solutions of the Refined Zigzag Theory [14,15]. These results serve as normalizing factors for the solutions presented in Table 4 and Figs. 12–18 (see Tables B1–B3).

References

[1] Timoshenko S. On the correction for shear of differential equations for transverse vibrations of prismatic bars. Philos Mag Ser 1921;41:744–6.
[2] Madabhusi-Raman P, Davalos JF. Static shear correction factors for laminated rectangular beams. Composites; Part B 1996;27B:285–93.
[3] Reddy JN. Mechanics of laminated composite plates and shells. Theory and analysis. 2nd ed. Boca Raton: CRC Press; 2004.
[4] Averill RC. Static and dynamic response of moderately thick laminated beams with damage. Compos Eng 1994;4(4):381–95.
[5] Averill RC, Yip YuenCheong. Development of simple, robust finite elements based on refined theories for thick laminated beams. Comput Struct 2006;59(3):529–46.
[6] Di Sciuva M. Development of an anisotropic, multilayered, shear-deformable rectangular plate element. Compos Struct 1985;21(4):789–96.
[7] Di Sciuva M. An improved shear-deformation theory for moderately thick multilayered anisotropic shells and plates. ASME J Appl Mech 1987;54:589–96.
[8] Di Sciuva M. Further refinement in the transverse shear deformation theory for multilayered composite plates. Atti Accademia delle Scienze di Torino 1990;124(5–6):248–68.
[9] Di Sciuva M. Multilayered anisotropic plate models with continuous interlaminar stresses. Compos Struct 1992;22(3):149–68.
[10] Cho M, Parmenter RR. An efficient higher order plate theory for laminated composites. Compos Struct 1992;20(2):113–23.
[11] Lu X, Liu D. An interlaminar shear stress continuity theory for both thin and thick composite laminates. ASME J Appl Mech 1992;59:502–9.
[12] Cho M, Parmenter RR. Efficient higher order composite plate theory for general lamination configurations. AIAA J 1993;31(7):1299–306.
[13] Tessler A, Di Sciuva M, Gherlone M. A refined linear zigzag theory for composite beams: reformulation of zigzag function and shear stress constraints. In: VI International symposium on advanced composites and applications for the new millennium, Corfu, Greece; 2007.
[14] Tessler A, Di Sciuva M, Gherlone M. Refinement of Timoshenko beam theory for composite and sandwich beams using zigzag kinematics. NASA/TP-2007-215086; 2007.
[15] Tessler A, Di Sciuva M, Gherlone M. A refined zigzag beam theory for composite and sandwich beams. J Compos Mater 2009;43(9):1051–81.
[16] Tessler A, Di Sciuva M, Gherlone M. A shear-deformation theory for composite and sandwich plates using improved zigzag kinematics. In: 9th International conference on computational structures technology, proceedings on CD, paper no. 30, Athens, Greece; September 2008.
[17] Tessler A, Di Sciuva M, Gherlone M. Refined zigzag theory for laminated composite and sandwich plates. NASA/TP-2009-215561; 2009.
[18] Tessler A, Di Sciuva M, Gherlone M. A consistent refinement of first-order shear-deformation theory for laminated composite and sandwich plates using improved zigzag kinematics. J Mech Mater Struct 2010;5(2):341–67.
[19] Tessler A, Di Sciuva M, Gherlone M. Refined zigzag theory for homogeneous, laminated composite, and sandwich plates: a homogeneous-limit methodology for zigzag function selection. NASA/TP-2010-216214; 2010.
[20] Tessler A, Di Sciuva M, Gherlone M. Refined zigzag theory for homogeneous, laminated composite, and sandwich plates: a homogeneous-limit methodology for zigzag function selection. Numer Methods Partial Differential Equations 2011;27(1):208–29.
[21] Hughes TJR, Taylor RL, Kanoknukulchai W. A simple and efficient element for plate bending. Int J Numer Methods Eng 1977;11:1529–43.
[22] Hughes TJR. The finite element method. Linear static and dynamic finite element analysis. NJ: Prentice-Hall; 1987 [chapter 5: The C^0-approach to plates and beams].
[23] Zienkiewicz OC, Taylor RL. The finite element method for solid and structural mechanics. 6th ed. Elsevier; 2005 [chapter 12].
[24] Tessler A, Dong SB. On a hierarchy of conforming Timoshenko beam elements. Comput Struct 1981;14:335–44.
[25] Tessler A. An efficient, conforming axisymmetric shell element including transverse shear and rotary inertia. Comput Struct 1982;15(5):567–74.
[26] Tessler A, Hughes TJR. A three-node Mindlin plate element with improved transverse shear. Comput Methods Appl Mech Eng 1985;50:71–101.
[27] Tessler A. A priori identification of shear locking and stiffening in triangular Mindlin elements. Comput Methods Appl Mech Eng 1985;53:183–200.
[28] Tessler A. Shear-deformable, anisoparametric flexure elements with penalty relaxation. In: Hughes TJR, Hinton E, editors. Finite element methods in plate and shell structures. London: Pineridge Press; 1986 [chapter 11].
[29] Tessler A, Spiridigliozzi L. Curved beam elements with penalty relaxation. Int J Numer Methods Eng 1986;23:2245–62.

[30] Fried I, Johnson AR, Tessler A. Minimum-degree thin triangular plate and shell bending finite elements of order two and four. Comput Methods Appl Mech Eng 1986;56:283–307.

[31] Tessler A, Spiridigliozzi L. Resolving membrane and shear locking phenomena in curved shear-deformable axisymmetric shell elements. Int J Numer Methods Eng 1988;26:1071–86.

[32] Tessler A. A C^0-anisoparametric three-node shallow shell element. Comput Methods Appl Mech Eng 1990;78:89–103.

[33] Barut A, Madenci E, Tessler A. Nonlinear elastic deformations of moderately thick laminated shells subjected to large and rapid rigid-body motion. Finite Elem Anal Des 1996;22:41–57.

[34] Barut A, Madenci E, Tessler A. Nonlinear analysis of laminates through a Mindlin-type shear deformable shallow shell element. Comput Methods Appl Mech Eng 1997;143:155–73.

[35] Barut A, Madenci E, Tessler A, Starnes JH. A new stiffened shell element for geometrically nonlinear analysis of composite laminates. Comput Struct 2000;77:11–40.

[36] Liu J, Riggs HR, Tessler A. A four-node, shear-deformable shell element developed via explicit Kirchhoff constraints. Int J Numer Methods Eng 2000;49:1065–86.

[37] Barut A, Madenci E, Tessler A. Nonlinear thermoelastic analysis of composite panels under non-uniform temperature distribution. Int J Solids Struct 2000;37:3681–713.

[38] Tessler A. Comparison of interdependent interpolations for membrane and bending kinematics in shear-deformable shell elements. In: Proceedings of international conference on computational engineering and sciences, Los Angeles, CA; 2000.

[39] Guzzafame D. Finite element formulation for the analysis of multilayered plates in cylindrical bending. M.S. thesis, Politecnico di Torino; October 2006.

[40] Fasano C. Development and implementation of interface techniques for beam finite elements. M.S. thesis (in Italian), Politecnico di Torino; March 2008.

[41] Oñate E, Eijo A, Oller S. Two-noded beam element for composite and sandwich beams using Timoshenko theory and Refined Zigzag Kinematics. Publication CIMNE No-346; October 2010.